Characterization of Surface Texture-Measuring Optical Microscopes using a Binary Pseudo-Random Array Standard

Ulf Griesmann [a], Keiko Munechika [b], T. Brian Renegar [a], X. Alan Zheng [a], Johannes A. Soons [a], Thomas A. Germer [a], Weilun Chao [c], Ian Lacey [d], Carlos Pina-Hernandez [b], Peter Z. Takacs [e], and Valeriy V. Yashchuk [d]

[a]National Institute of Standards and Technology (NIST) Gaithersburg, MD 20899-8211, USA

[b]HighRI Optics Inc., 5401 Broadway Terrace, St. 304, Oakland, CA 94618, USA

[c]Center for X-Ray Optics, Lawrence Berkeley National Laboratory, Berkeley, CA 94720, USA

[d]Advanced Light Source, Lawrence Berkeley National Laboratory, Berkeley, CA 94720, USA

[e]Surface Metrology Solutions LLC, 19 1st St S, Minneapolis, MN 55401 USA

ABSTRACT

Accurate topography measurements of engineered surfaces over a wide range of spatial frequencies are required in many applications. The instrument transfer function (ITF) of the microscope used to characterize the surface topography must be taken into consideration to ensure that the height, or depth, of features with higher spatial frequency content is not underestimated. This applies especially when comparing surface topography measurements made by different types of microscopes. We discuss ITF measurements of a confocal microscope and an interferometric microscope using a binary pseudo-random array (BPRA) standard. BPRA standards are surfaces designed to have constant power spectral density (PSD) over the spatial frequency range of a microscope. The ITF of a microscope can thus be derived from a PSD measurement of a BPRA standard in a straight-forward manner. We further show how BPRA standards can be used as efficient diagnostic tools to characterize aspects of the imaging performance of topography-measuring microscopes.

Keywords: surface topography measurement, instrument transfer function, binary pseudo-random array standard

1. INTRODUCTION

For areal topography measurements with optical microscopes of complex surfaces that are characterized by a wide range of spatial frequencies and slopes, the spatial frequency response of the topography measuring microscope

Author e-mail: ulf.griesmann@nist.gov

must be considered, because optical instruments generally lose sensitivity with increasing spatial frequency. (This equally applies to other types of imaging instruments.) Insofar as a topography measuring microscope can be described as a shift-invariant linear system, its response to the spatial frequency content of a surface can be described with an instrument transfer function (ITF), which specifies the amplitude attenuation of sinusoidal surface components for every possible spatial frequency in the bandpass of the microscope (for a review see Ref. 1). For complex surfaces, especially surfaces that have high spatial frequencies and slopes, knowledge of the ITF may be needed to correctly interpret the topography measured by a microscope. Knowledge of a microscope's ITF is especially important when measurements from different classes of topography microscopes are compared because they may have substantially different instrument transfer functions.

Surface topography metrology has in recent years seen the development and standardization of methods for the performance characterization of topography measuring microscopes, which is, for example, evident in the International Organization for Standardization (ISO) 25178 series of documentary standards.[2] Standardized areal reference artifacts, or material measures, suitable for the characterization of topography microscopes (see ISO 25178-70[3]) are now becoming commercially available.[4–6] Existing standards offer ways to estimate the resolution of topography microscopes or even map the instrument transfer function. An example are the areal measures with star-shape grooves (ASG) described in ISO 25178-70. Alternatively, a step artifact can be used for the estimation of the instrument transfer function.[1,7] However, a consensus regarding the best method for determining instrument transfer functions has yet to emerge.

In this paper we discuss the application of a binary pseudo-random array (BPRA) standard,[8–10] which is a surface engineered to have uniform spatial frequency content in the bandpass of a topography microscope, to estimate the instrument transfer function of two different topography microscopes. We also demonstrate how a BPRA standard can be used as a check standard for a topography microscope to determine, for example, if the microscope is set up and aligned correctly.

2. BINARY PSEUDO-RANDOM ARRAY STANDARDS

Binary pseudo-random array (BPRA) surfaces designed to have a "white" spatial frequency spectrum were first proposed by Yashchuk *et al.*as standards for the transfer function estimation of several types of scientific imaging instrumentation.[8–13] The design of a BPRA surface proceeds from the insight that a surface with constant spatial frequency content must have a delta function-like autocorrelation, because the power spectral density of such a surface, which is the Fourier transform of the autocorrelation, will have a constant value for all spatial frequencies. (This is a form of the well-known Wiener-Khinchin theorem.)

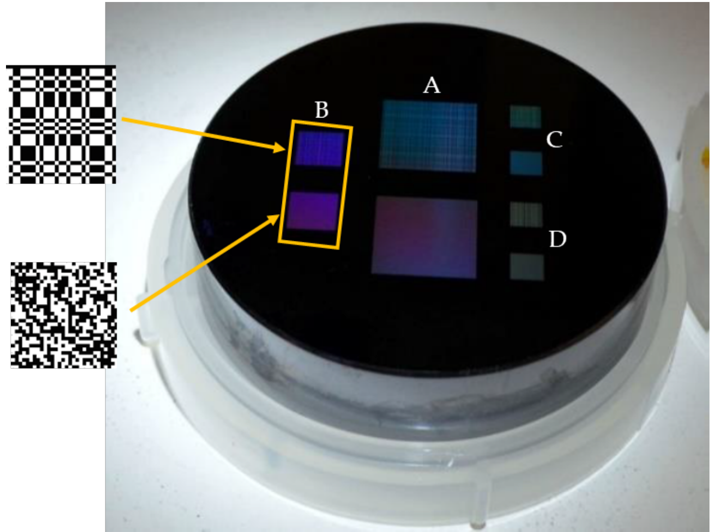

Figure 1: Binary pseudo-random array (BPRA) standard used in the present investigation. The substrate is a super-polished disc of silicon with 50.8 mm diameter and a thickness of 12.7 mm. The standard contains four pairs of patterns, each consisting of a uniformly random array (top pattern) and a binary pseudo-random array (bottom pattern). The elementary pixel width is 2.5 µm for patterns A, 1.2 µm for patterns B, 0.8 µm for patterns C, and 0.4 µm for patterns D. All areas have a size of close to 4000 × 4000 pixels. The height of the patterns is approximately 35 nm.

An engineer wishing to design a surface with delta function-like autocorrelation is faced with the problem that the surface features, and thus the autocorrelation spike, cannot be made arbitrarily small. An elementary, finite feature size must be chosen that is determined partly by the process used for the surface fabrication and by optical considerations that will be discussed in Section 3. Thus, one way to construct a surface with spike-like autocorrelation is to choose an elementary pixel size and construct a binary array of pixels that satisfies the desired autocorrelation condition. The choice of binary arrays has two advantages. The first is that it immediately suggests lithographic processes for the fabrication of BPRA, which are ideally suited for the fabrication of binary patterns with small feature sizes. The other advantage is that the designer can draw on a large body of work on matrices with perfect autocorrelation, which have applications in several imaging and image processing applications[14–17] (here and in the following sections "autocorrelation" refers to the cyclical autocorrelation).

The first realizations of two-dimensional patterns with perfect autocorrelation for transfer function estimation described by were based on the uniformly random arrays (URA) developed by Fenimore and Cannon[15] for aperture coded x-ray imaging. While uniformly random arrays have perfect autocorrelation they are less well

suited for applications in microscopy because it is often impossible to image the entire array with a microscope if it is not specifically designed to match the field of view.[12] A sub-array of a URA, however, does not have perfect autocorrelation and, thus, not the desired uniform spatial frequency spectrum.

An alternative to URAs is to use highly randomized pseudo-random arrays that are generated by sequentially filling rows, or columns, of the pixel matrix from a sequence of pseudo-random bits with equal number of "0" and "1" bits. Alternatively, a physical random bit generator could be used to fill the matrix.[18] Highly randomized binary pseudo-random arrays are self-similar in the sense that both the whole arrays *and their sub-arrays* have the necessary spike-like autocorrelation. The instrument transfer function $\mathcal{T}(\xi)$, where ξ is the spatial frequency, of a topography microscope is obtained by first measuring a BPRA standard surface, and then calculating the power spectral density $S(\xi)$.[19–21] If the assumption holds that the intrinsic power spectral density of the BPRA standard surface, $\bar{S}(\xi)$, is constant as designed,[22] the ITF can be calculated from the observed power spectral density $S(\xi)$ because

$$S(\xi) = \bar{S}(\xi) \cdot |\mathcal{T}(\xi)|^2. \tag{1}$$

All measurements discussed in Sec. 3 were made using the BPRA standard shown in Fig. 1. This standard has four URA and BPRA pairs with different elementary pixel sizes. For patterns A the elementary pixel width is 2.5 µm, it is 1.2 µm for patterns B, 0.8 µm for patterns C, and 0.4 µm for patterns D. All areas have a size of approximately 4000×4000 pixels. The height of all patterns is approximately 35 nm.[23] The URA pattern areas were not used in the measurements shown here.

3. MICROSCOPY EXAMPLES

We demonstrate the utility of BPRA standards for instrument transfer function estimation by comparing measurements of the standard shown in Figs. 1 made with an optical coherence scanning interferometric (CSI) microscope and a confocal microscope. For the comparison of the two microscopes, both microscopes used objectives with a nominal magnification of 20. The Mirau objective on the CSI microscope has a numerical aperture (NA) of 0.4, whereas the NA of the confocal microscope's objective is 0.6.

3.1 Coherence scanning interferometric microscope

Figure 2 shows the power spectral density derived from topography measurements made with the CSI microscope for three of the BPRA areas on the BPRA standard. PSDs are plotted both with a logarithmic spatial frequency scale in Fig. 2a and also with a linear spatial frequency scale to more clearly show the behavior of the PSD curves at higher spatial frequencies in Fig. 2b. PSDs are plotted for frequencies ranging from the lowest frequency determined by the field of view of the microscope up to the Nyquist frequency determined by the sampling of the

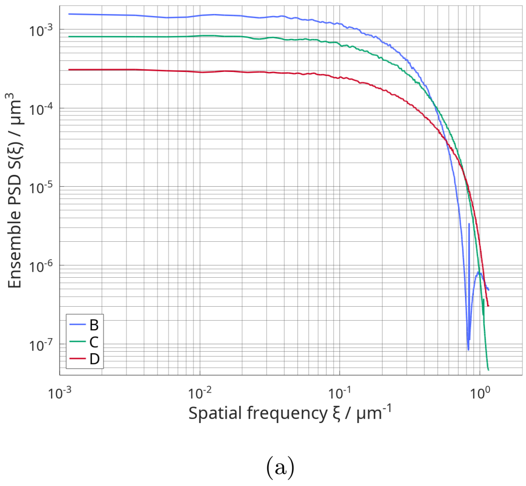

(a)

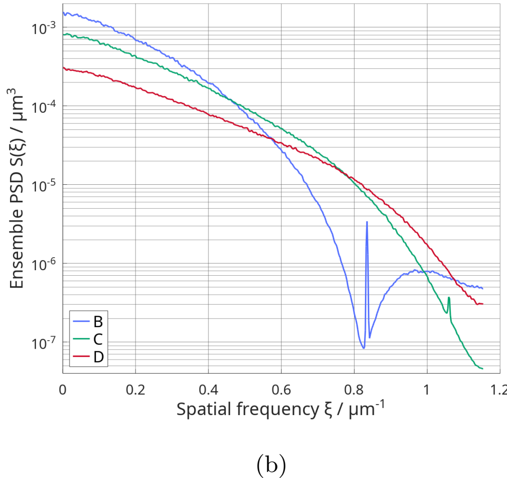

(b)

Figure 2: Power spectral densities of the highly randomized binary pseudo-random array areas on the standard shown in Fig. 1, measured with an interferometric microscope. The microscope objective had a numerical aperture of 0.4 and an image magnification of 20. A logarithmic scale is used for the spatial frequency in (a), whereas a linear scale is used in (b). The highest frequency in the plot is the Nyquist frequency of the image sensor.

image sensor. The PSD curves in Figs. 2a and 2b were obtained by first calculating the PSD for each horizontal and vertical pixel line in the way described by Church and Takacs[20] (using a Blackman window). This was followed by averaging of all profile PSDs because the profile PSDs in horizontal and vertical direction were found to be identical. The resulting ensemble PSDs for BPRA areas B, C, and D are shown in Figs. 2. The elementary pixel size for area B is 1.2 µm, well above the Abbe diffraction limit of about 0.75 µm for the effective microscope wavelength of 0.597 µm and the numerical aperture of 0.4. The PSD curves in Fig. 2 for the BPRA area B are thus the product of the measured PSD of the BPRA surface that is multiplied with a sinc^2 function, the Fourier transform of the elementary pixel profile. The minimum value of the sinc^2 factor, however, does not extend to 0 due to the effective apodization of the elementary pixel shape resulting from the finite pixel size of the image sensor. For BPRA area C the pixel size of 0.8 µm is still above the Abbe limit and the PSD curves in Figs. 2 for area C are still affected by diffraction off the elementary pixels. Only for BPRA D is the elementary pixel size of 0.4 µm below the Abbe diffraction limit and we can assume that the shapes of the PSD curves for area D in Fig. 2 result solely from the transfer function of the microscope.

In the PSD for BPRA area B shown in Fig. 2 a prominent spike occurs near the minimum in the PSD. We developed a simple model of the microscope measurement which takes simulates the sampling of the BPRA standard by the image sensor of the microscope. This enables us to explore the effect of fabrication errors that may affect the BPRA surface.

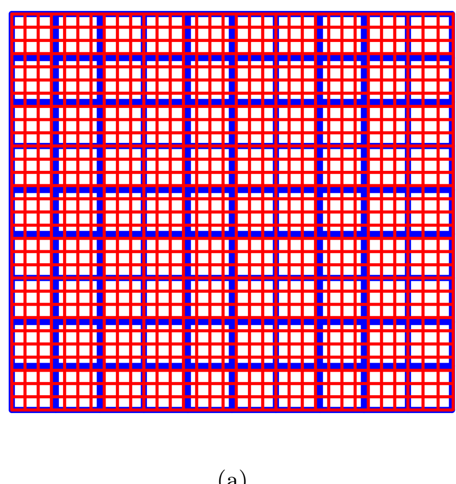

(a)

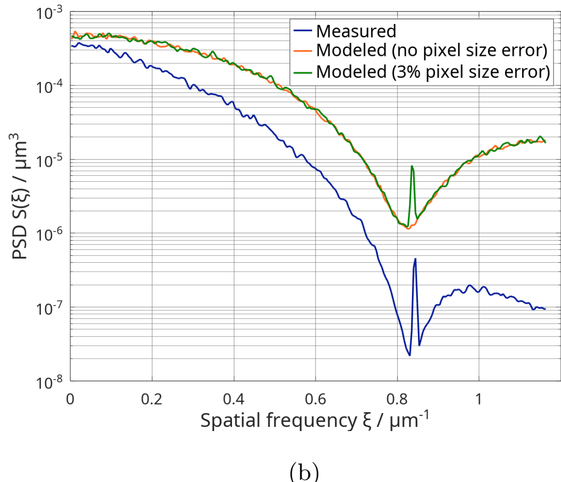

(b)

Figure 3: (a) Comparison of BPRA elementary pixel size of 1.2 µm for patterns B (see Fig. 1) shown as a blue grid (thick lines), and the sensor pixel size of 0.43 µm for the interferometric microscope with the 20× magnification objective shown as a red grid (thin lines). (b) Modeled PSD for the pixel sizes shown in (a).

Figure 3a illustrates the sampling of the BPRA area B by the image sensor of the CSI microscope with the 20× magnification objective. The elementary pixel size for area B is 1.2 µm which is indicated in Fig. 3a using a grid of blue lines. For the microscope objective with 20× magnification the sensor pixel spacing ("pixel size") is 0.43 µm. The sensor pixel size is indicated in Fig. 3a with a grid of red lines. The ratio of BPRA pixel size to the sensor pixel size is 2.791 or, in good approximation, 67/24. The sampling of the BPRA area by the sensor of the microscope was simulated by first dividing each BPRA pixel of a BPRA array into 67 ×67 sub-pixels and then averaging the values in 24 ×24 sub-pixel areas, thus replicating the sampling of BPRA area B with the microscope at 20× magnification. The PSD of the resulting sampled BPRA surface is shown in Fig. 3b together with the PSD of the measured BPRA area B. The PSD of the model resembles the measured PSD except that it appears shifted upward because it does not contain the effect of the microscope's ITF and the spike that is observed in the measured PSD is not present in the PSD of the modeled measurement.

Next, we simulated a fabrication error by removing a single pixel from the the pixel areas of the 67-times expanded BPRA array before averaging the 24×24 pixel blocks. For an isolated pixel this corresponds to a reduction in pixel size by about 3%. When the BPRA area is fabricated, a reduction in pixel size can occur, for example, by an exposure dose error during lithographic patterning. When the PSD is calculated from a BPRA area with reduced pixel size, a spike appears that is very similar to the one seen in the PSD of the actual BPRA area B (see Fig. 3), and which is not present in the PSD of the perfect BPRA pattern.

Having established that the BPRA area D has a pixel size that makes it suitable for the illumination wave-

length of the CSI microscope, we can use it to estimate the instrument transfer properties of the microscope with objectives that have different magnifications. Fig. 4 shows the PSD curves of topography measurements of the BPRA standard area D made with Mirau objectives having magnifications of 10 (NA = 0.3, 0.87 µm/pixel), 20 (NA = 0.4, 0.43 µm/pixel), and 50 (NA = 0.55, 0.17 µm/pixel). In the measurement that was made with the 10× objective, the system error of the CSI microscope was inadvertently not subtracted from the measured topography, which is the cause for the raised PSD at the lowest frequencies. In the PSD curve for the measurement with the 50× objective we notice an uncharacteristically sharp drop of the PSD with increasing spatial frequency such that the PSD becomes essentially zero even for frequencies below the Nyquist frequency. This behavior could be traced to a mis-alignment of the objective. A Mirau objective must be aligned such that when the surface under test is in focus the optical path difference in the two arms of the Mirau interferometer is zero. When the measurement shown in Fig. 4 was made, the objective had drifted out of alignment so that the BPRA surface was not in focus at the zero path difference point of the objective. The results in Fig. 4 thus show that the BPRA standard is an efficient and sensitive tool to check the proper alignment and function of a CSI microscope.

3.2 Confocal microscope

A reflectance-mode confocal microscope in a configuration similar to the CSI microscope described in Sec. 3.1 was also evaluated with the BPRA standard shown in Fig. 1. As with the CSI microscope, measurements were made

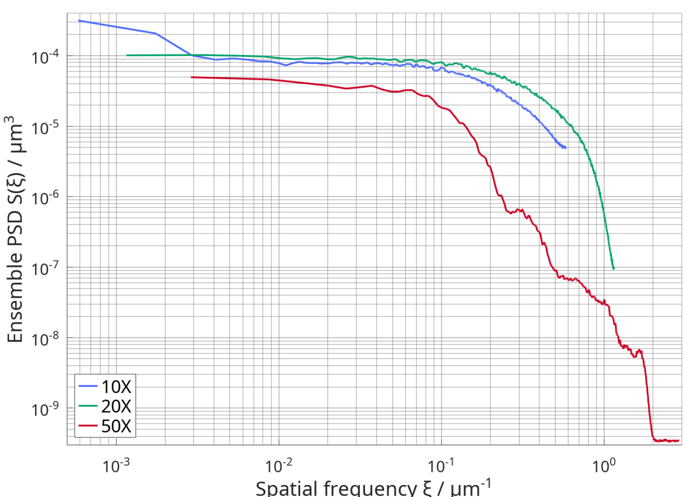

Figure 4: Power spectral densities of BPRA area D with 0.4 µm elementary pixel size on the standard shown in Fig. 1, measured with an interferometric microscope using three different objectives with magnifications 10, 20, and 50.

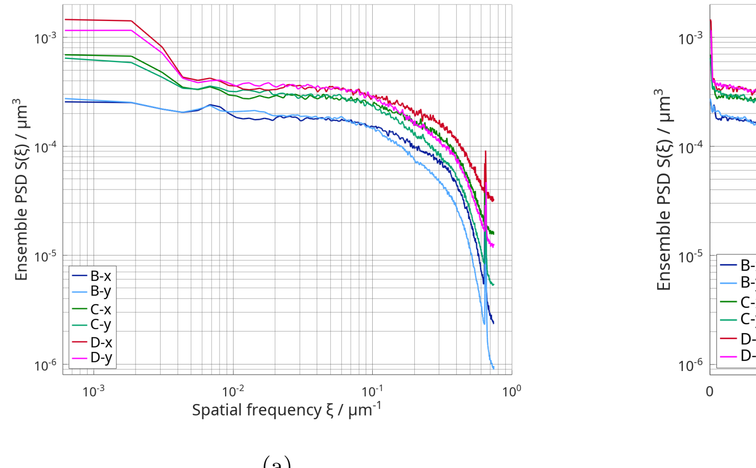

(a)

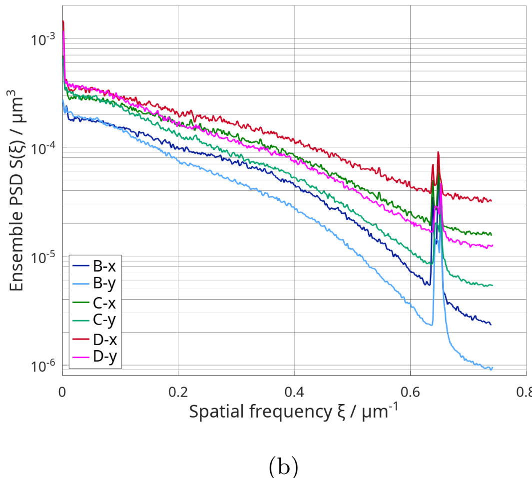

(b)

Figure 5: Power spectral densities of the binary pseudo-random array areas on the standard shown in Fig. 1, measured with a spinning Nipkow disk confocal microscope. The microscope objective had a numerical aperture of 0.6 and an image magnification of 20. A logarithmic scale is used for the spatial frequency in (a), whereas a linear scale is used in (b).

of the BPRA areas B, C, and D. The results for the PSD calculated from the topography measurements are shown in Fig. 5. Ensemble PSD curves were calculated for pixel lines in horizontal (x) and vertical (y) direction because we found a pronounced difference in the PSD for the two sensor directions. This difference can likely be traced to the spinning disk sampling mechanism used in the confocal microscope in which the sampling in one direction is determined by the hole spacing in the disk and in the other direction is limited by the electronic sampling rate. The electro-mechanical scanning mechanism also causes arcuate features in the topography measurements that have very low frequency and vary in amplitude, which result in the elevated PSD at the low frequency end of the PSD curves shown in Fig. 5. The spatial frequency bandpass of the confocal microscope is narrower than that of the CSI microscope discussed in Sec. 3.1, so that the Fourier transform of the pixel is less evident in the PSD curves for the BPRA areas B and C. The spikes near the high spatial frequency end of all PSD curves in Fig. 5 must be an artifact caused by the microscope. The cause is currently not known. A surprising result of the measurements with the confocal microscope is that the resolution of the instrument is clearly inferior to that of the CSI microscope even though the numerical aperture of the confocal microscope's objective is substantially larger. Again, we can see that a single measurement of a BPRA standard can produce a wealth of information regarding the performance of a topography microscope.

4. TOWARDS MATERIAL MEASURES FOR MICROSCOPE ITF CALIBRATION

In the words of ISO 25178-70,[3] a material measure (calibration standard) is a "dedicated manufactured workspace intended to reproduce or supply, in a permanent manner during its use quantities of one or more given kinds, each with an assigned quantity value", which can be used for "calibration of the metrological characteristics, followed by assessment of the measurement uncertainty" or "user adjustment of the instrument, which establishes corrections of the measured quantities". BPRA standards are promising candidates for material measures that provide the user with a "white" spatial frequency spectrum over a specified spectral range suitable for efficient and robust estimation of a topography microscope's instrument transfer function and related quantities, such as the point spread function and resolution. With the examples discussed in Secs. 3.1 and 3.2 we have demonstrated that BPRA standards can also be used to evaluate the performance characteristics of topography measuring microscopes, to perfect the adjustment of the instrument, and, potentially, to correct measured surface topographies using an estimated ITF.

There remain, however, open questions relating to the assessment of the measurement uncertainty. Again, in the words of ISO 25178-70: "The material characteristics of the material measure shall not significantly affect the measurement carried out on it." Fabrication processes used to make BPRA surfaces are imperfect and may result in fabrication errors that affect the spatial frequency spectrum of the BPRA surface. For example, surfaces patterned with electron beam lithography may have "stitching errors" due to the step-and-expose process in which many small sub-areas are exposed sequentially. In addition to patterning errors, a surface may have height errors, or the pattern height may be non-uniform across the pattern, or, as we have shown, the patterns may have errors in the size of the elementary pixels. The effect of fabrication errors on the BPRA surface spectrum needs to be quantified as part of an uncertainty statement for the spatial frequency spectrum. Work in this area is ongoing. For example, initial measurements have been made to show that two nominally identical BPRA standards that were fabricated separately have the same PSD[24] when measured with the same CSI microscope. The goal of these efforts is to establish the uncertainty of the spatial frequency spectrum which, in turn, would make it possible to assign an uncertainty to a measured PSD, or ITF.

Acknowledgments

We gratefully acknowledge financial support by the Forensics Program of the NIST Special Programs Office, through United States Department of Energy (DOE) contract DE-AC02-05CH11231, and through Small Business Innovation Research (SBIR) award 80NSSC20C0505 to HighRI Optics, Inc. from the National Aeronautic and Space Administration (NASA).

REFERENCES

[1] de Groot, P. J., "The instrument transfer function for optical measurements of surface topography," *J. Phys. Photonics* **3**, 024004 (2021).

[2] International Organization for Standardization (ISO), [*ISO 25178 – Geometrical Product Specifications*].

[3] International Organization for Standardization (ISO), [*ISO 25178 Geometrical Product Specifications – Surface texture: Areal – Part 70: Material measures*] (2014).

[4] Leach, R. K., Giusca, C. L., and Rubert, P., "A single set of material measures for the calibration of areal surface topography measuring instruments: the npl areal bento box," in [*Proceedings of the 14th International Conference on Metrology and Properties of Engineering Surfaces, 17-21 June 2013, Taipei, Taiwan*], (2013).

[5] Eifler, M., Hering, J., von Freymann, G., and Seewig, J., "Calibration sample for arbitrary metrological characteristics of optical topography measuring instruments," *Optics Express* **26**, 16609–16623 (2018).

[6] Eifler, M., Hering, J., Leach, R. K., von Freymann, G., Hu, X., and Dai, G., "Comparison of material measures for areal surface topography measuring instrument calibration," *Surf. Topogr.: Metrol. Prop.* **8**, 025019 (2020).

[7] Zhang, X., Kashti, T., Kella, D., Frank, T., Shaked, D., Ulichney, R., Fischer, M., and Allebach, J. P., "Measuring the modulation transfer function of image capture devices: what do the numbers really mean?," *Proc. SPIE* **8293**, 829307 (2012).

[8] Yashchuk, V. V., McKinney, W. R., and Takacs, P. Z., "Binary pseudorandom grating as a standard test surface for measurement of modulation transfer function of interferometric microscopes," *Proc. SPIE* **6704**, 670408 (2007).

[9] Yashchuk, V. V., McKinney, W. R., and Takacs, P. Z., "Binary pseudorandom grating standard for calibration of surface profilometers," *Opt. Eng.* **47**, 073602–1–5 (2008).

[10] Yashchuk, V. V., McKinney, W. R., and Takacs, P. Z., "Test surfaces useful for calibration of surface profilometers," (2013). Patent No.: US 8,616,044.

[11] Barber, S. K., Anderson, E. D., Cambie, R., McKinney, W. R., Takacs, P. Z., Stover, J. C., Voronov, D. L., and Yashchuk, V. V., "Binary pseudo-random gratings and arrays for calibration of modulation transfer functions of surface profilometers," *Nucl. Instr. Methods. Phys. Res. A* **616**, 172–182 (2010).

[12] Yashchuk, V., Babin, S., Cabrini, S., Chao, W., Griesmann, U., Lacey, I., Marchesini, S., Munechika, K., Pina-Hernandez, C., and Roginsky, A., "Binary pseudorandom array test standard optimized for characterization of large field-of-view optical interferometers," in [*Interferometry XX*], *Proc. SPIE* **11490**, 200–207, SPIE (2020).

[13] Munechika, K., Cabrini, S., Chao, W., Lacey, I., Pina-Hernandez, C., Rochester, S., and Yashchuk, V. V., "Binary pseudo-random array test standard optimized for characterization of interferometric microscopes," in [*Applied Optical Metrology IV*], Novak, E., Trolinger, J. D., and Wilcox, C. C., eds., **11817**, 10 – 19, International Society for Optics and Photonics, SPIE (2021).

[14] Calabro, D. and Wolf, J. K., "On the synthesis of two-dimensional arrays with desirable correlation properties," *Information and Control* **11**, 537–560 (1968).

[15] Fenimore, E. E. and Cannon, T. M., "Coded aperture imaging with uniformly redundant arrays," *Appl. Opt.* **17**, 337–347 (1978).

[16] Gottesman, S. R. and Fenimore, E. E., "New family of binary arrays for coded aperture imaging," *Appl. Opt.* **28**, 4344–4352 (1989).

[17] Svalbe, I. D. and Tirkel, A. Z., "Extended families of 2d arrays with near optimal auto and cross correlation," *EURASIP J. Adv. Signal Process.* **18** (2017).

[18] Wahl, M., Leifgen, M., Berlin, M., Röhlicke, T., and Rahn, H.-J., "An ultrafast quantum random number generator with provably bounded output bias based on photon arrival time measurements," *Appl. Phys. Lett.* **98**, 171105 (2011).

[19] Church, E. L. and Takacs, P. Z., "Effect of the optical transfer function in surface profile measurements," *Proc. SPIE* **1164**, 46–59 (1989).

[20] Church, E. L. and Takacs, P. Z., "Optimal estimation of finish parameters," *Proc. SPIE* **1530**, 71–85 (1991).

[21] Elson, J. M. and Bennett, J. M., "Calculation of the power spectral density from surface profile data," *Appl. Opt.* **34**, 201–208 (1995).

[22] Takacs, P. Z., Rochester, S., Lacey, I., Munechika, K., and Yashchuk, V. V., "Calibration, modeling, parameterization, and verification of the instrument transfer function of an interferometric microscope," *Proc SPIE* **12223**, 1222308 (2022).

[23] Munechika, K., Rochester, S., Chao, W., Lacey, I., Pina-Hernandez, C., and Yashchuk, V. V., "Binary pseudo-random array standards for calibration of 3d optical surface profilers used for metrology with aspheric x-ray optics," *Proc. SPIE* **12223**, 1222307 (2022).

[24] Yashchuk, V. V., Munechika, K., Rochester, S., Chao, W., Lacey, I., Pina-Hernandez, C., and Takacs, P., "Reliability investigation of the instrument transfer function calibration technique based on binary pseudo-random array standards," *Proc. SPIE* **12240**, 1224025 (2022).